Bremsstrahlung from hot, dense, partially ionized plasmas

R. Kawakami and K. Mima
Institute of Laser Engineering, Osaka University, Suita, Osaka, 565, Japan

H. Totsuji and Y. Yokoyama
Department of Electronics, Okayama University, Tsushimanaka, Okayama, 700, Japan
(Received 25 March 1988)

In hot, dense, and partially ionized plasmas, both the electronic shielding and the ion-ion correlation modify the emission and absorption coefficients of the bremsstrahlung. Based on the Thomas-Fermi model and the hypernetted-chain equation, it has been shown that the emission and absorption coefficients are significantly reduced by these effects.

I. INTRODUCTION

The energy transport by radiation is one of the most important problems in laser fusion plasmas. Since the parameters of laser plasmas such as density and temperature cover very wide domains, the radiative transport coefficients for various plasma parameters are needed in order to describe the hydrodynamics of matter and radiation in laser plasmas. In these parameter domains, we have the cases where the electronic shielding and/or the ion-ion correlation significantly modify the x-ray emission and absorption coefficients of the free-state–free-state and bound-state–free-state transitions.

The typical x-ray radiation intensity emitted from high-Z plasmas is $\sim 10^{13}-10^{14}$ W/cm^2 or $\sim 100-180$ eV in terms of the radiation temperature. When a solid target is irradiated by the x ray, the hot dense plasma is produced on the surface. An example of the temperature, density, and pressure profiles at 1 ns after irradiation of the aluminum foil of thickness 20 μm is shown in Fig. 1. The density and temperature of these plasmas are $\sim 10^{22}-10^{23}$ cm^{-3} and $\sim 30-100$ eV, respectively, and the average charge state of Al ion Z^* is $\sim 4-8$. For these plasmas, the coupling parameter of the ion is estimated as $\Gamma=(Z^*e)^2/a_0k_BT=2-10$ and the degeneracy parameter $E_F/k_BT=0.1-1$. Here a_0 is the average ion radius $(3/4\pi n_i)^{1/3}$, E_F is the Fermi energy at zero temperature $\hbar^2(3\pi^2 n_e)^{2/3}/2m$, n_i and n_e are the number density of electron and ion, respectively, and m is the electron mass. The purpose of this paper is to discuss high density effects on the x-ray interaction with those plasmas.

The previous paper[1] by one of the authors showed that the ion-ion correlation reduces the free-state–free-state emission and absorption cross sections in fully ionized low-Z plasmas ($Z<5$). In this paper we extend this work to such partially ionized medium or high-Z plasmas ($Z>5$) as shown in Fig. 1. Both free and bound electrons screen the ionic Coulomb field to reduce the electron-ion collision cross section in those plasmas. Therefore the electronic shielding together with the ion-ion correlation reduce the x-ray emission and absorption cross section.

The bremsstrahlung is proportional to Z^{*2}, when ions are assumed to be point charges of Z^* and not correlated with each other. The reduction factor $(Z^*/Z)^2$ describes the bound electronic shielding effect. However the real ion has the finite size a_b which corresponds to the outermost radius of the bound electron orbit. Therefore, when the impact parameter for the electron-ion collision b is smaller than a_b, the effective ion charge for collision $Z_{\rm eff}$ will be greater than Z^*. Actually, when b is much smaller than a_b, the colliding electron feels the bear ion charge Z. Since the average frequency of the emitted or absorbed radiation is roughly estimated to be $\hbar/(2mb^2)$ as will be discussed in Sec. VI, $Z_{\rm eff}$ of the free-state–free-state transition increases with the frequency. The details of this dependence is closely related to the electronic shielding and the ion-ion correlation.

We determine the shielded electrostatic potential around the ion by the finite temperature Thomas-Fermi model.[2,3] In this model, the other ions are considered as the uniform positive charge background of which charge state is Z^*. The effect of the ion-ion correlation is taken

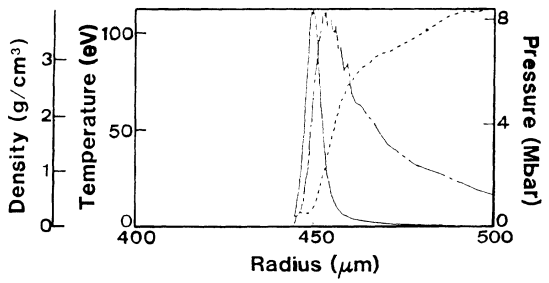

FIG. 1. Density, temperature, and pressure profiles at 1 ns after irradiation of the Al foil of thickness 20 μm. The radiation is Planckian and its temperature is 140 eV. The solid line shows density, the dotted line shows temperature, and the dashed line is the pressure.

into account as in Ref. 1. Note here that the average ion model (or the average charge state Z^*) is applicable only when Z is sufficiently larger than unity. Otherwise, the charge state fluctuation is comparable to Z^* and the Thomas-Fermi potential (the average ion potential) is not valid.[4]

In Sec. II we derive the emission and absorption coefficients absorption cross section. Section III describes the case where the electron-ion correlation is weak and the linear response theory is applicable. Section IV is devoted to the evaluation of the Thomas-Fermi potential. In Sec. V we describe the numerical analysis of the hypernetted-chain (HNC) equation for the screened ion-ion interaction. Finally the discussions and summary are given in Sec. VI.

II. FORMULATION

The cross section for dipole emission of photon is given by[5]

$$d\sigma_{kp'}=\frac{(2\pi)^2}{\omega^3}\frac{m}{\hbar p}\left|\mathbf{e}^*\cdot\left[\frac{d^2\mathbf{d}}{dt^2}\right]_{fi}\right|^2\delta(E_i-E_f-\hbar\omega)\times\frac{d\mathbf{k}}{(2\pi)^3}\frac{d\mathbf{p}'}{(2\pi)^3}\ . \tag{1}$$

Here $\mathbf{e}$ and $\mathbf{k}$ are the polarization and the wave number of the emitted photon, respectively, $\omega=(c^2k^2+\omega_p^2)^{1/2}$, $\omega_p^2=4\pi n_e e^2/m$, and $(d^2\mathbf{d}/dt^2)_{fi}$ is the matrix element of the time derivative of the electronic dipole moment $\mathbf{d}$ between the initial state [energy $E_i=(\hbar p)^2/2m$ and asymptotic wave number $\mathbf{p}$] and the final state [energy $E_f=(\hbar p')^2/2m$ and asymptotic wave number $\mathbf{p}'$] of the electron. When the electron position is $\mathbf{r}(t)$,

$$\frac{d^2\mathbf{d}}{dt^2}=e\frac{d^2\mathbf{r}}{dt^2}=\frac{e^2}{m}\sum_{j=1}^{N_i}\nabla U(|\mathbf{r}-\mathbf{R}_j|)\ , \tag{2}$$

and the matrix element is given as follows:

$$\left[\frac{d^2\mathbf{d}}{dt^2}\right]_{fi}=\frac{e^2}{m}\int\Psi_f^*(r)\left[\frac{\partial}{\partial\mathbf{r}}\sum_{j=1}^{N_i}U(|\mathbf{r}-\mathbf{R}_j|)\right]\Psi_i(r)d\mathbf{r}\ . \tag{3}$$

Here $U(r)$ is the ion potential shielded by free and bound electrons which is determined later by the Thomas-Fermi analysis, $\mathbf{R}_j$ $(j=1,2,\ldots,N_i)$ is ion position, and N_i is the number of ions.

In the Born approximation, the cross section averaged over the ion distribution, the polarization, and the propagation direction of photon is calculated as

$$\overline{d\sigma_{kp'}}=\frac{Z^2e^6}{3\pi^2mc^3\hbar p\omega^2q^2}(\omega^2-\omega_p^2)^{1/2}n_iS(q)P(q)\times\delta(E_i-E_f-\hbar\omega)d\omega\,d\mathbf{p}'\ , \tag{4}$$

where $\hbar\mathbf{q}=\hbar\mathbf{p}-\hbar\mathbf{p}'$ is the change of the electronic momentum in the collision, $S(q)$ is the structure factor of the ion defined by

$$S(q)=\left\langle\left|\sum_{j=1}^{N_i}\exp(i\mathbf{q}\cdot\mathbf{R}_j)\right|^2\right\rangle/N_i\ , \tag{5}$$

and $P(q)$ is the shielding factor,

$$P(q)=\left|\frac{q^2}{4\pi Ze}\int U(r)e^{-i\mathbf{q}\cdot\mathbf{r}}d\mathbf{r}\right|^2\ . \tag{6}$$

The emission coefficient $E(\omega)d\omega$ (energy emitted per unit time, volume, solid angle, and polarization) is given by

$$E(\omega)d\omega=\int\int\hbar\omega\frac{\hbar p}{m}\overline{d\sigma_{kp'}}f(p)[1-f(p')]\frac{2}{(2\pi)^3}d\mathbf{p}\ , \tag{7}$$

where $f(p)$ is the distribution function of free electrons with momentum $\hbar p$,

$$f(p)=1\Big/\left[1+\exp\frac{(\hbar p)^2/2m-\mu}{k_BT}\right]\ , \tag{8}$$

and μ is the chemical potential. Carrying out the integration with respect to $\mathbf{p}$ and $\mathbf{p}'$ in Eq. (7) we get

$$E(\omega)d\omega=\frac{2Z^2e^6}{3\pi^3c^3\hbar^3\omega}\frac{1}{\exp(\hbar\omega/k_BT)-1}\times(\omega^2-\omega_p^2)^{1/2}n_ik_BT\,d\omega\times\int_0^\infty S(q)P(q)F(q)\frac{1}{q}dq\ , \tag{9}$$

where

$$F(q)=\ln\frac{1+\exp\left[\frac{\mu}{k_BT}-\frac{\hbar^2}{2mk_BT}\left[\frac{q}{2}-\frac{m\omega}{\hbar q}\right]^2\right]}{1+\exp\left[\frac{\mu}{k_BT}-\frac{\hbar^2}{2mk_BT}\left[\frac{q}{2}+\frac{m\omega}{\hbar q}\right]^2\right]}\ . \tag{10}$$

From the emission cross section, the absorbed power density (absorbed energy per unit time, volume, solid angle and polarization) is given by

$$Q(\omega)d\omega=\int\int\hbar\omega\frac{\hbar p}{m}N_k\overline{d\sigma_{kp'}}\times\{f(p')[1-f(p)]-f(p)[1-f(p')]\}\frac{2}{(2\pi)^3}d\mathbf{p}\ , \tag{11}$$

where N_k is the photon number. We then obtain the absorption coefficient $A(\omega)$ by the same procedure as Eq. (9),

$$A(\omega)=\frac{Q(\omega)d\omega}{\hbar\omega N_k(\omega^2-\omega_p^2)d\omega/8\pi^3c^2}=\frac{16Z^2e^6}{3c\hbar^4\omega^2(\omega^2-\omega_p^2)^{1/2}}n_ik_BT\times\int_0^\infty S(q)P(q)F(q)\frac{1}{q}dq\ . \tag{12}$$

As in Ref. 1, we introduce the ratio $R(\omega)$ by

$$R(\omega)=\frac{E(\omega)[S(q),P(q)]}{E(\omega)[S(q)=P(q)=1]}=\frac{A(\omega)[S(q),P(q)]}{A(\omega)[S(q)=P(q)=1]}=\frac{\int_0^\infty S(q)P(q)F(q)\frac{1}{q}dq}{\int_0^\infty F(q)\frac{1}{q}dq}\ . \tag{13}$$

Furthermore, the following ratios:

$$R_i(\omega)=\frac{E(\omega)[S(q),P(q)=1]}{E(\omega)[S(q)=P(q)=1]}=\frac{A(\omega)[S(q),P(q)=1]}{A(\omega)[S(q)=P(q)=1]}=\frac{\int_0^\infty S(q)F(q)\frac{1}{q}dq}{\int_0^\infty F(q)\frac{1}{q}dq}\ , \tag{14}$$

$$R_e(\omega)=\frac{E(\omega)[S(q)=1,P(q)]}{E(\omega)[S(q)=P(q)=1]}=\frac{A(\omega)[S(q)=1,P(q)]}{A(\omega)[S(q)=P(q)=1]}=\frac{\int_0^\infty P(q)F(q)\frac{1}{q}dq}{\int_0^\infty F(q)\frac{1}{q}dq} \tag{15}$$

are introduced to express the ion-ion correlation effect and the electronic shielding effect separately.

III. EFFECTS OF THE ELECTRON SHIELDING ON THE FREE-FEEE TRANSITION FOR WEAK ELECTRON-ION CORRELATION (WEAK SCREENING)

When the electron-ion correlation is not strong, the response of electrons to the ionic Coulomb field may be described by the linear response theory. (The condition for weak electron-ion correlation will be discussed in Sec. VI.) The Fourier component of the ionic Coulomb potential $4\pi Ze/q^2$ is then replaced by $4\pi Ze/q^2\epsilon_e(q)$, where $\epsilon_e(q)$ is the dielectric function of electrons. The value of

$$\int_0^\infty S(q)P(q)F(q)\frac{1}{q}dq$$

in Eqs. (9), (12), and (13) is thus evaluated as

$$\int_0^\infty S(q)F(q)\frac{1}{q\epsilon_e^2(q)}dq\ , \tag{16}$$

where $S(q)$ is structure factor for ions which interact via the screened Coulomb potential $4\pi Ze/q^2\epsilon_e(q)$.

For a given photon energy $\hbar\omega$, the dominant contribution to the integration of Eq. (16) comes from $q_{\max}\sim(2m\omega/\hbar)^{1/2}$, namely, $q_{\max}/k_F\sim(\hbar\omega/E_F)^{1/2}$, where $F(q)$ becomes maximum. When the screening function $1/\epsilon_e(q)$ is sufficiently smaller than unity at $q=q_{\max}$, the photon emission and absorption cross sections are reduced by this screening. For an example, $F(q)$ and $F(q)/\epsilon_e^2(q)$ are compared for $k_BT/E_F=1$ in Fig. 2. Since the static screening is more effective for a smaller q, the low energy photon absorption and emission cross sections are significantly reduced.

On the other hand, the electronic screening reduces the effective coupling between ions and increase $S(q)$ for small q in comparison with case of no screening. This increase of $S(q)$ partially cancels the reduction due to the factor $1/\epsilon_e^2(q)$.

In order to see the above two effects separately, we introduce

$$R_1(\omega)=\frac{E(\omega)[S(q)=1,\epsilon_e(q)]}{E(\omega)[S(q)=\epsilon_e(q)=1]}=\frac{A(\omega)[S(q)=1,\epsilon_e(q)]}{A(\omega)[S(q)=\epsilon_e(q)=1]} \tag{17}$$

and

$$R_2(\omega)=\frac{E(\omega)[S(q),\epsilon_e(q)]}{E(\omega)[S(q)=1,\epsilon_e(q)]}=\frac{A(\omega)[S(q),\epsilon_e(q)]}{A(\omega)[S(q)=1,\epsilon_e(q)]}\ . \tag{18}$$

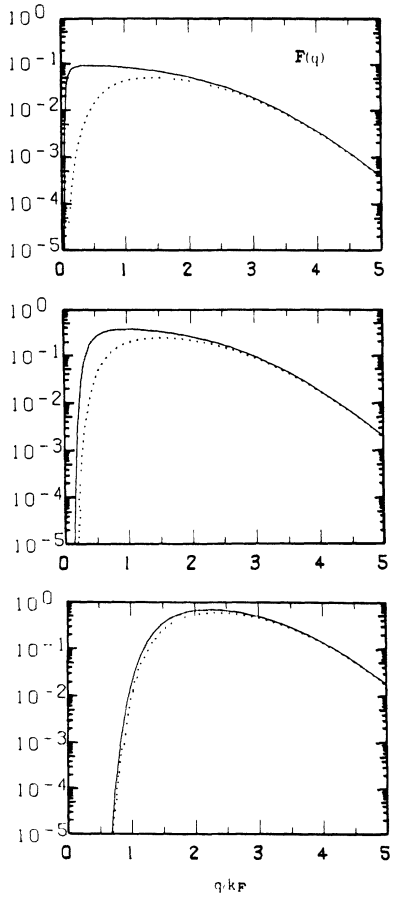

FIG. 2. Values of the factor $F(q)$ and $F(q)/\epsilon_e^2(q)$ with $k_BT=E_F$ are plotted by solid and dotted lines, respectively, for $\hbar\omega/k_BT=0.2$ (top), 1 (middle), and 5 (bottom). $k_F=(3\pi^2ne)^{1/3}$.

The ratio $R_1(\omega)$ is the measure of the electronic screening effects without the ion-ion correlation and the ratio $R_2(\omega)$ is the ion correlation effects. When we increase $r_s=(3/4\pi n_e)^{1/3}/a_B$ (where a_B is the Bohr radius) with the other parameters k_BT/E_F and Γ kept constant, the electronic screening becomes strong and we can see how strongly the emission and absorption cross sections are modified by the screening.

We have evaluated the ratios $R_1(\omega)$ and $R_2(\omega)$ adopting the random-phase approximation (RPA) for the dielectric response function of electrons: RPA may be used as the first approximation at least for smaller values of r_s. The values of $S(q)$ have been evaluated by linear interpolation between the results of numerical experiments of one-component plasma (OCP) ($r_s=0$) and the screened OCP (Ref. 6) for $r_s=1$: Almost the same values for $R_1(\omega)$ and $R_2(\omega)$ are obtained also when we use the solution of the HNC equation for screened OCP as $S(q)$.

Figures 3(a)–3(c) show $R_1(\omega)$, $R_2(\omega)$, and $R(\omega)=R_1(\omega)R_2(\omega)$ for various values of r_s. In Fig. 3(a) we see that $R_1(\omega)$ decreases when r_s increases from 0.1 to 1, $k_BT/E_F=1$ and $\Gamma=2$ being fixed. The electron density and temperature and the ion charge are related to r_s as shown in Table I. On the other hand, the ion correlation effect is reduced when r_s increases as in Fig. 3(b). Figure 3(c) shows that $R(\omega)=R_1(\omega)R_2(\omega)$ is almost independent of r_s. Namely, the decrease of $R_1(\omega)$ is almost canceled by the increase of $R_2(\omega)$. Therefore we may conclude that the electronic shielding effects are not significant as far as the weak screening approximation is valid.

Figures 4(a) and 4(b) show the case for $\Gamma=10$. Since the electronic screening effect does not depend on Γ, $R_1(\omega)$ is the same as Fig. 3(a). Again, the product of $R_1(\omega)$ and $R_2(\omega)$ does not depend on r_s as shown in Fig. 4(b). The modifications of the cross section are much more sensitive to the electron temperature as shown in Figs. 5(a)–5(c) where $\Gamma=2$ and $r_s=0.5$ are fixed and k_BT/E_F changes from 0.5 to 2.

Finally, let us discuss the validity of the static screening. The frequency dependence of the dielectric function $\epsilon_e(q,\omega)$ may become important when $\omega>qv_e$ for $k_BT>E_F$ or qv_F for $E_F>k_BT$, where v_e and v_F are the electron thermal velocity and the Fermi velocity. Since the important region of q is around $(2m\omega/\hbar)^{1/2}$, the above condition is rewritten as $\hbar\omega>3k_BT$ or $3E_F$. Namely, the static screening approximation may not be valid when $\hbar\omega>3k_BT$ or $\hbar\omega>3E_F$. As it is shown by Fig. 3(a), however, the effect of the electron screening becomes significant for $\hbar\omega<2-3E_F$ irrespective of the value of E_F/k_TT. Therefore, the static screening approximation will be acceptable as the first stage approximation.

IV. THE FINITE TEMPERATURE THOMAS-FERMI MODEL (STRONG SCREENING)

The electrostatic potential around an ion embedded in hot dense plasmas may be approximately evaluated by the Thomas-Fermi model. When Z is sufficiently large,

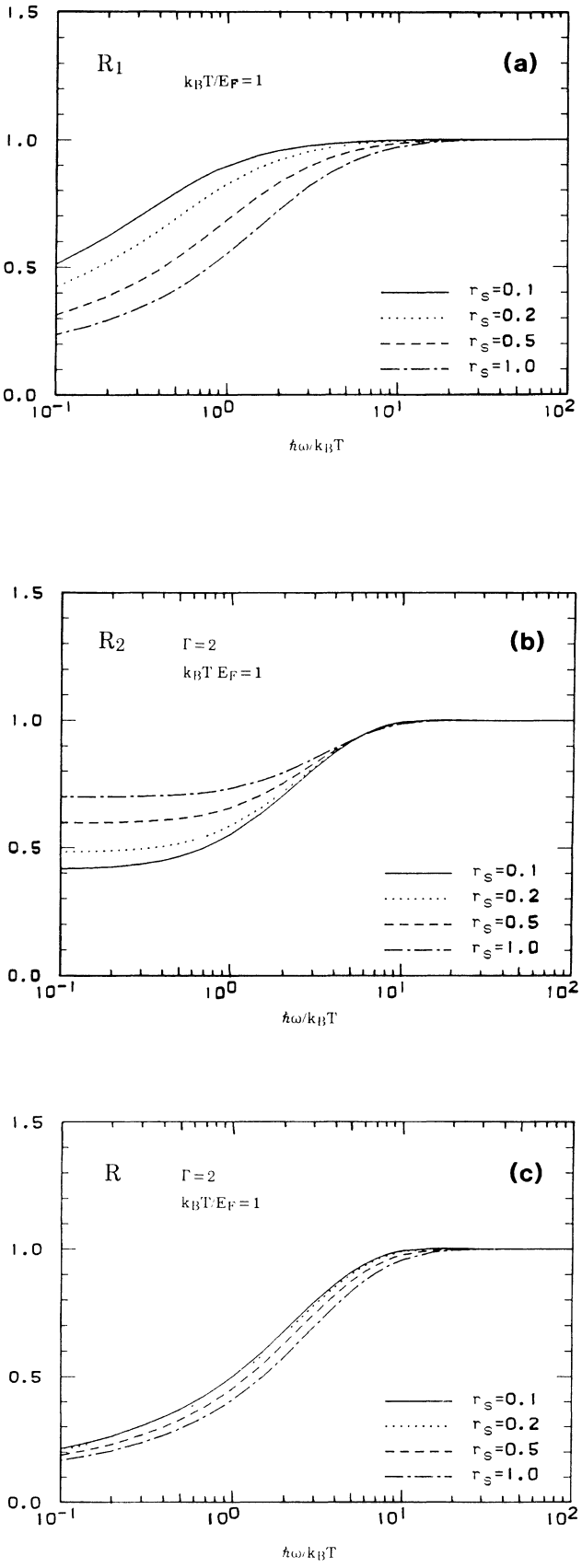

FIG. 3. Ratios (a) $R_1(\omega)$, (b) $R_2(\omega)$, and (c) $R(\omega)=R_1(\omega)R_2(\omega)$ for $k_BT/E_F=1$ and $\Gamma=2$.

TABLE I. Electron density, temperature, and atomic number for $\Gamma=2$, $k_B T=E_F$, and several values of r_s.

r_s	n_e (cm^{-3})	T (eV)	Z
0.1	1.6×10^{27}	5000	15
0.2	2.0×10^{26}	1250	9
0.5	1.3×10^{25}	200	4.5
1.0	1.6×10^{24}	50	2.7

the average ion potential gives a good approximation for the real ion potential in plasmas.

We assume that a test ion is placed in the electron gas of density Z^*n_i. The density and average charge of ions in the uniform positive charge background are n_i and Z^*e, respectively. Then the Thomas-Fermi potential $U(r)$ satisfies the following equations:

$$-\nabla^2 U(r)=4\pi e[Z\delta(r)-n_e(r)+Z^*n_i]\ , \tag{19}$$

$$n_e(r)=\int f_T(p)\frac{2}{(2\pi)^3}d\mathbf{p}\ , \tag{20}$$

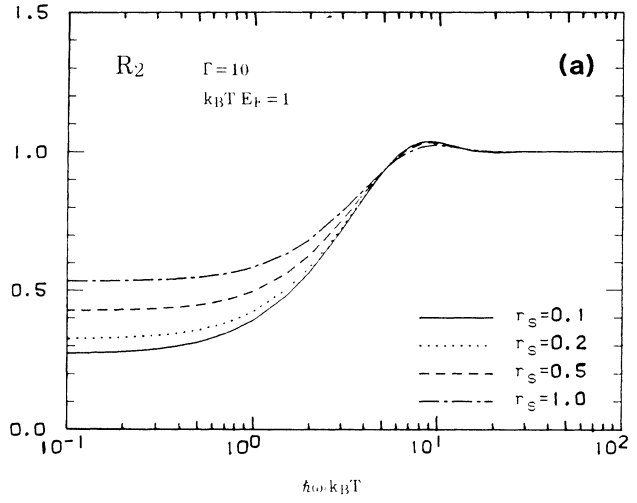

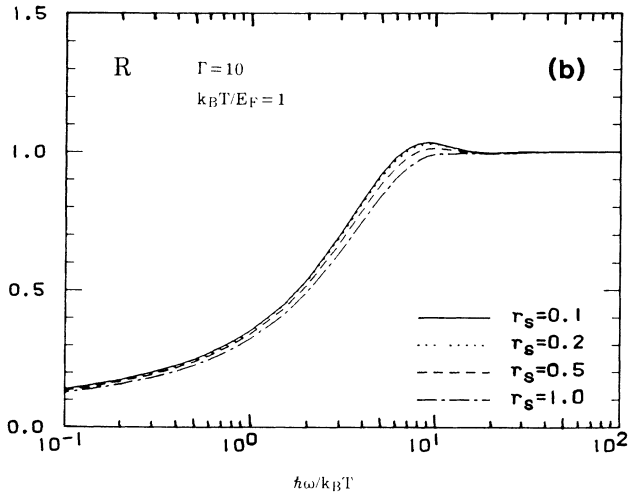

FIG. 4. Ratios (a) $R_2(\omega)$ and (b) $R(\omega)=R_1(\omega)R_2(\omega)$ for $\Gamma=10$, where $R_1(\omega)$ is the same as Fig. 3(a).

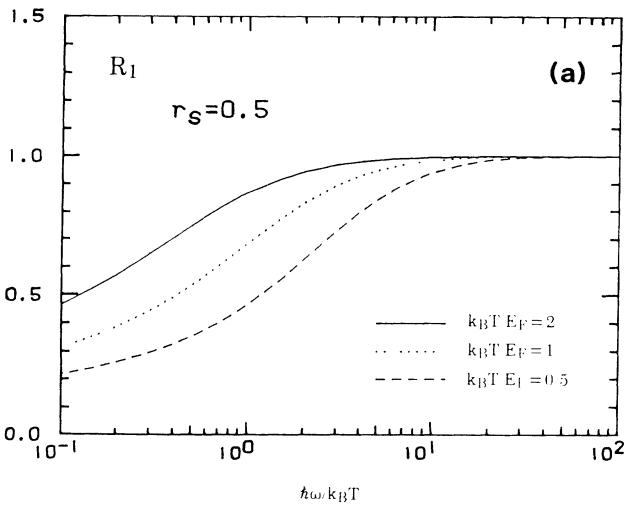

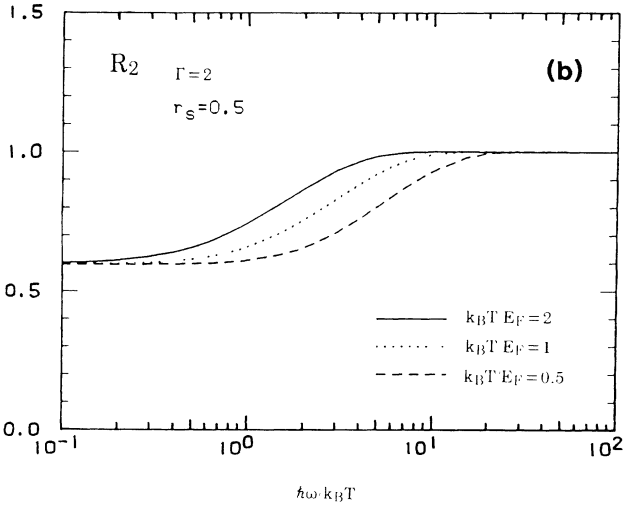

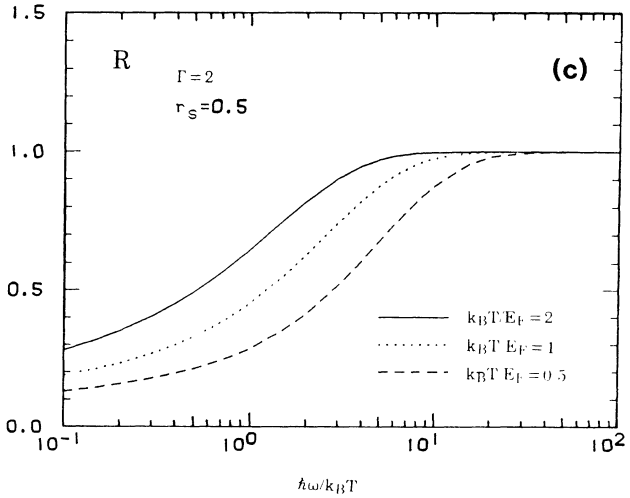

FIG. 5. Same as Figs. 3(a)–3(c) for $r_s=0.5$ and $\Gamma=2$.

and

$$f_T(p)=1\Big/\left[1+\exp\frac{(\hbar p)^2/2m-eU(r)-\mu}{k_BT}\right] . \quad (21)$$

We have numerically solved these equations under the boundary conditions,

$$\frac{dU(r)}{dr}=-\frac{Ze}{r^2}\quad (r\to 0),\quad U(r)=\frac{C}{r}e^{-r/\lambda}\quad (r\to\infty) . \quad (22)$$

Here C is an unknown constant which is determined after integrating Eq. (19) with the conditions and (22), and λ is the Thomas-Fermi shielding distance given by

$$\lambda^{-2}=\frac{4\sqrt{2}m^{3/2}e^2}{\pi\hbar^3}k_BT^{1/2}\int_0^\infty\frac{y^{1/2}e^{y-\mu/k_BT}}{(1+e^{y-\mu/k_BT})^2}dy . \quad (23)$$

When $k_BT\to\infty$, λ is reduced to the Debye shielding distance.

In order to determine the average ion charge state Z^* self-consistently with the Thomas-Fermi model, we regard the electron with negative energies as the bound electron of the test ion at $r=0$. Then the number of the bound electrons, $N_{\rm BE}$, is given by

$$N_{\rm BE}=\int_0^\infty 4\pi r^2 n_{\rm BE}(r)dr , \quad (24)$$

where

$$n_{\rm BE}(r)=\int_{p^2/2m-eU(r)<0}f_T(p)\frac{2}{(2\pi)^3}d\mathbf{p} , \quad (25)$$

and we obtain

$$Z^*=Z-N_{\rm BE} . \quad (26)$$

Since Z^*n_i is equal to the average free-electron density,

$$Z^*n_i=\int f(p)\frac{2}{(2\pi)^3}d\mathbf{p} . \quad (27)$$

Equation (27) relates the average ion charge state Z^* to the chemical potential μ.

In order to define Z^* by Eq. (26), the spatial spread of the bound electron around the test ion a_b must be smaller than the ion sphere radius a_0, which is one half of the average distance between ions; otherwise, the bound state wave functions of neighboring ions overlap and the negative energy electrons can move from one ion to another. The bound electron profiles given in Figs. 6(a) and 6(b) show that the bound electron radius a_b defined by $n_{\rm BE}(a_b)=Z^*n_i$ is sufficiently smaller than a_0, and justify the definition of Z^* by Eq. (26).

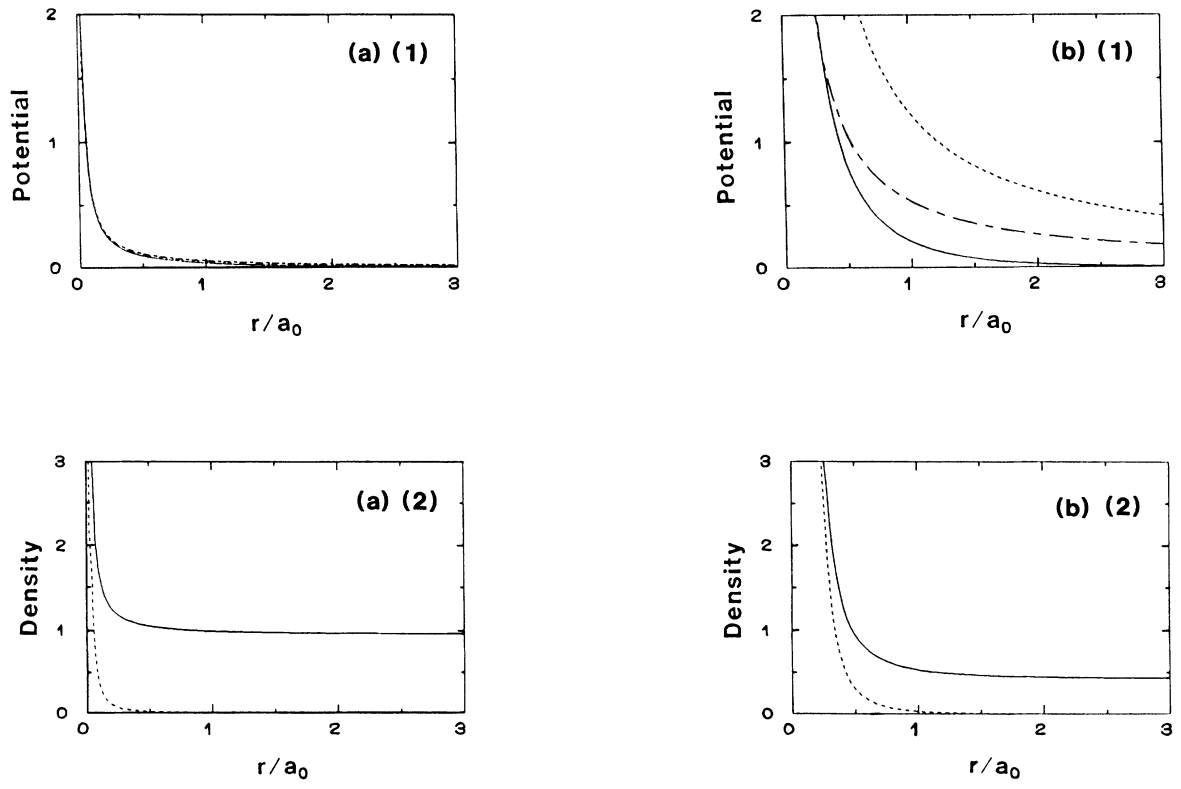

FIG. 6. (a) Profiles of some quantities of the Thomas-Fermi model for case (a). In (1), the solid line shows the Thomas-Fermi potential $eU(r)/rk_BT$, the dotted line shows Ze^2/rk_BT, and the dashed-dotted line shows Z^*e^2/rk_BT. In (2), the solid and dotted lines show, respectively, the total electron density and the bound electron density normalized by the average electron density Z^*n_i. (b) same as (a) for the case (b).

V. THE HYPERNETTED-CHAIN EQUATION FOR THE SCREENED ION-ION INTERACTION

When the Coulomb coupling between ions becomes comparable with the kinetic energy of the ion, or $\Gamma \sim 1$, the Debye-Hückel model is no longer applicable. The ion correlations in such high density plasmas are described by some integral equations. Since we are interested in the parameter region of $1 < \Gamma < 10$, we may employ the hypernetted-chain (HNC) equation which is known to work as a good approximation when the ionic coupling parameter is not so large.[7] The HNC equation is given by

$$1+h(r)=\exp\left[-\frac{\Phi_{ii}(r)}{k_B T}+h(r)-c(r)\right], \tag{28}$$

supplemented by the Ornstein-Zernike relation

$$h(r)=c(r)+n_i\int c(|\mathbf{r}'-\mathbf{r}|)h(r')d\mathbf{r}', \tag{29}$$

where $c(r)$ is the direct correlation function. The radial distribution function of the ion $g(r)$ and the structure factor $S(q)$ are related to $h(r)$ as

$$g(r)=1+h(r), \tag{30}$$

$$S(q)=1+n_i\int h(r)e^{i\mathbf{q}\cdot\mathbf{r}}d\mathbf{r}. \tag{31}$$

We note that the binary interaction potential $\Phi_{ii}(r)$ is not well defined, because both bound and free electrons shield the ion potential and modify $\Phi_{ii}(r)$ which is given by Z^2e^2/r without electronic shielding. Two limiting cases may be as follows. In the first case, the ion of charge state Z^* feels the Thomas-Fermi potential $U(r)$ given in Sec. IV, namely, $\Phi_{ii}(r)=Z^*U(r)$. In the second case, $\Phi_{ii}(r)=ZU(r)$. When $r/a_b \gg 1$, the bound electron orbits do not overlap between the interacting ions and each ion is assumed to be a point charge of Z^*e. Therefore the interaction potential is well approximated by the first case. When $r/a_b \ll 1$, on the other hand, the bound electron orbits overlap significantly and the interacting ion charge can be approximated by the nuclear charge Ze. Therefore $\Phi_{ii}(r)$ may be given by the second case. Since a_b is sufficiently smaller than a_0, we employ $\Phi_{ii}(r)=Z^*U(r)$ to calculate absorption coefficients.

VI. DISCUSSIONS AND SUMMARY

We here discuss the results of foregoing analyses in the following two cases. In case (a), the parameters are $Z=13$, $n_i=8\times10^{21}$ cm^{-3}, and $k_BT=1$ keV. In case (b), $Z=13$, $n_i=8\times10^{22}$ cm^{-3}, and $k_BT=100$ eV.

The profiles of the potential, total electron density, and bound electron density obtained by the Thomas-Fermi equations are shown in Figs. 6(a) and 6(b). In case (a) shown by Fig. 6(a), the aluminum ion is almost fully ionized and the ion charge is shielded only by free electrons. In this case the average interaction energy between electron and ion Ze^2/a_e, where $a_e=(3/4\pi Z^*n_i)^{1/3}$, satisfies the condition $Ze^2/a_e \ll k_BT$, and the potential $U(r)$ is close to the Debye-Hückel potential: The condition of weak electron-ion correlation may be satisfied if either $Ze^2/a_e \ll k_BT$ or $Ze^2/a_e \ll E_F$. On the other hand, there is significant amount of bound electrons in case (b) shown by Fig. 6(b) and the ion charge is strongly shielded: In this case, $Ze^2/a_e \gg k_BT$.

Note here that the present Thomas-Fermi model has a uniform positive charge background since we have to treat the electron-ion and ion-ion correlations separately in order to evaluate the bremsstrahlung. Therefore the average charge state Z^* for Figs. 6(a) and 6(b) are different from the ion charge which is obtained from the Thomas-Fermi equations based on the ion sphere model (average ion model). In Fig. 7 the relation between Z^* and the ion density of our model are compared with that of the average ion model.[2]

The radial distribution functions of the ion $g(r)$ obtained by the HNC equation[7] are shown in Figs. 8(a) and 8(b), where the results for two assumptions for the binary interaction potentials described in Sec. V and also the case of bare potential for comparison. We see that the ion correlation becomes stronger for larger binary interactions. Hence the ion-ion correlation is significantly reduced when electrons shield the potential.

In order to evaluate the emission coefficient $E(\omega)$ and the absorption coefficient $A(\omega)$, we have to calculate the structure factor $S(q)$, the shielding factor $P(q)$, and the factor $F(q)$. The wave-number dependence of these quantities are shown in Fig. 9(a) and 9(b). If ions do not correlate with each other and there is no electronic shielding, then $g(r)=1$ and $U(r)=Ze/r$, or $S(q)=P(q)=1$. When ion correlations and electronic screening are taken into account, the values of $S(q)$ and $P(q)$ become smaller than unity. From Eqs. (9) and (12), we obtain $E(\omega)$ and $A(\omega)$, shown in Figs. 10(a) and 10(b) in comparison with the case of $S(q)=P(q)=1$. We see that these coefficients are significantly reduced. It should be noted that the degeneracy of electron leads to reduced coefficients by itself[1,8] and the modification of $S(q)$ and $P(q)$ gives further reduction.

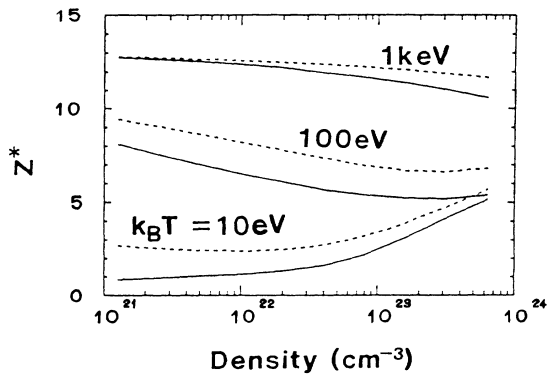

FIG. 7. Average charge state for ion density and temperature. The solid line shows the result of our model and the dotted line is that of the average ion model.

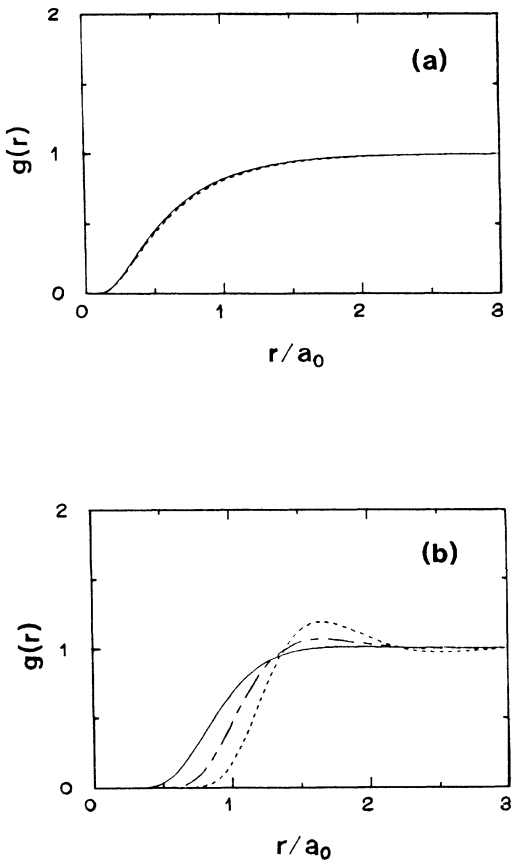

FIG. 8. Radial distribution function of ions for case (a). The solid line shows the result when $\Phi_{ii}(r)=Z^*eU(r)$, the dotted line shows $ZeU(r)$, the dashed-dotted line shows Z^2e^2/r. (b) Same as (a) for case (b).

To analyze the effects of the electron shielding and the ion-ion correlation on the bremsstrahlung quantitatively, we have introduced $R(\omega)$, $R_i(\omega)$, and $R_e(\omega)$ by Eqs. (13), (14), and (15), respectively. Their values are shown in Figs. 11(a) and 11(b). When we can assume an ion to be a point charge of Z^*e and not correlated with each other, the value of $R(\omega)$ is constant and equals to $(Z^*/Z)^2$ because the bremsstrahlung is proportional to the square of the ion charge state. Comparing $R_i(\omega)$ and $R_e(\omega)$ for case (b), we see that $R_e(\omega)$ indicating the electron shielding effect is very close to $R(\omega)$. Therefore the reduction of the bremsstrahlung is dominated by the electron shielding in Fig. 11(b). But when k_BT and/or E_F are large enough, ions are almost fully ionized. In this case, both the bound and free electrons have weak screening effects on the charge and the ion-ion correlation effect is dominant in the bremsstrahlung. This situation may be seen in Fig. 11(a) for case (a).

We may interpret the difference of $R(\omega)$ from the value $(Z^*/Z)^2$ in Figs. 11(a) and 11(b) for $\hbar\omega/k_BT>1$ as follows. High energy photons ($\hbar\omega>k_BT$) from the bremsstrahlung are emitted from the electron-ion collisions with a small impact parameter. The effect impact parameter for the emission of the photon of $\hbar\omega$ can be

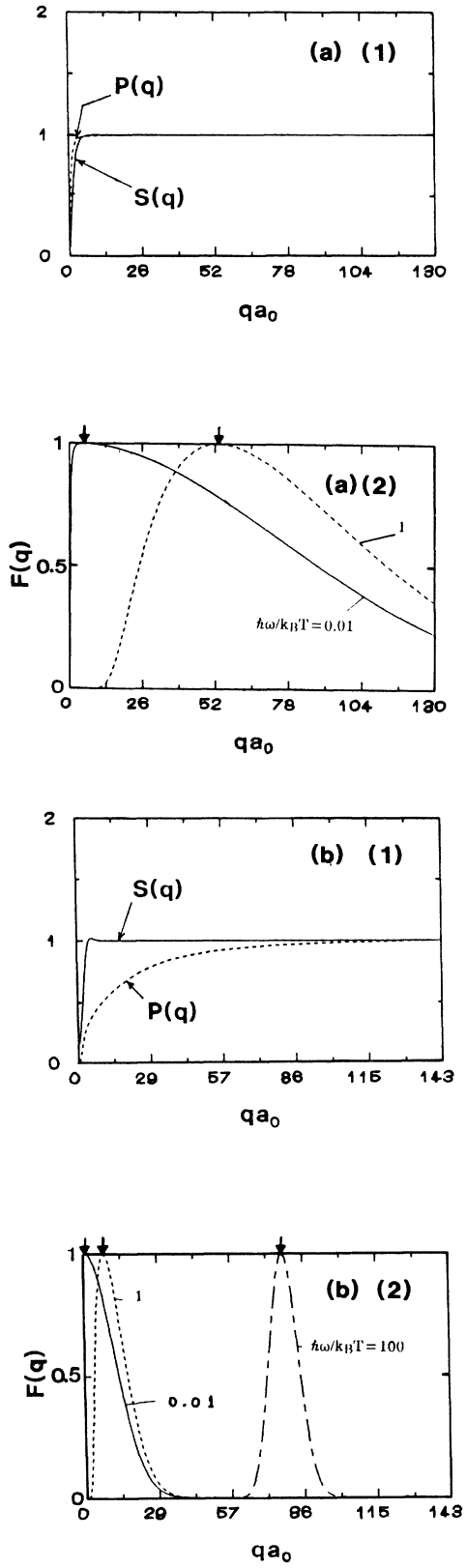

FIG. 9. (a) Structure factor $S(q)$, the shielding factor $P(q)$, and $F(q)$ for case (a). In (1), the solid lines shows $S(q)$ and the dotted line shows $P(q)$. In (2), we show $F(q)$ for $\hbar\omega/k_BT=0.01$, 1, and 100. The value of $F(q)$ is normalized by its maximum for each parameter. (b) Same as (a) for case (b).

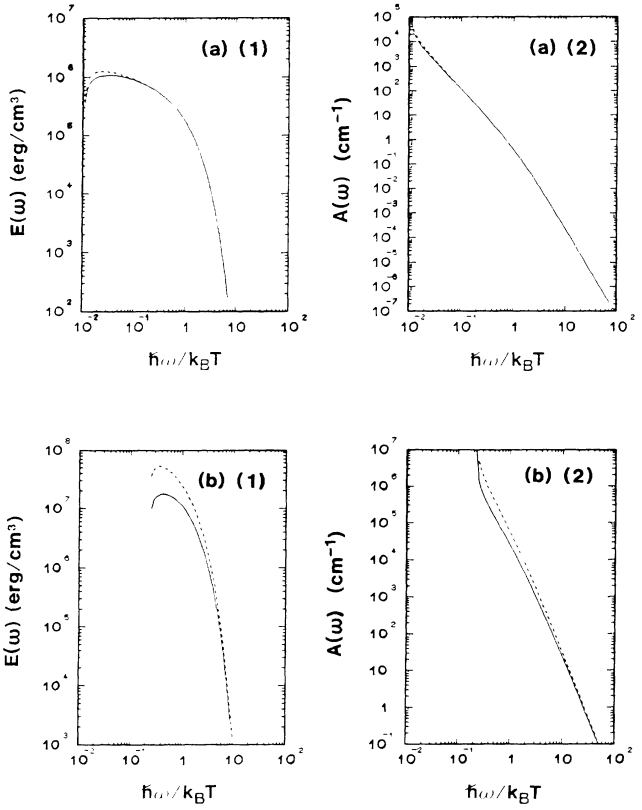

FIG. 10. (a) Emission and absorption coefficients for case (a). The solid line represents the results obtained by calculating $S(q)$ and $P(q)$, while the dotted line gives the values when there is no electron shielding and ions do not correlate with each other, namely, $S(q)=P(q)=1$. (b) Same as (a) for the case (b).

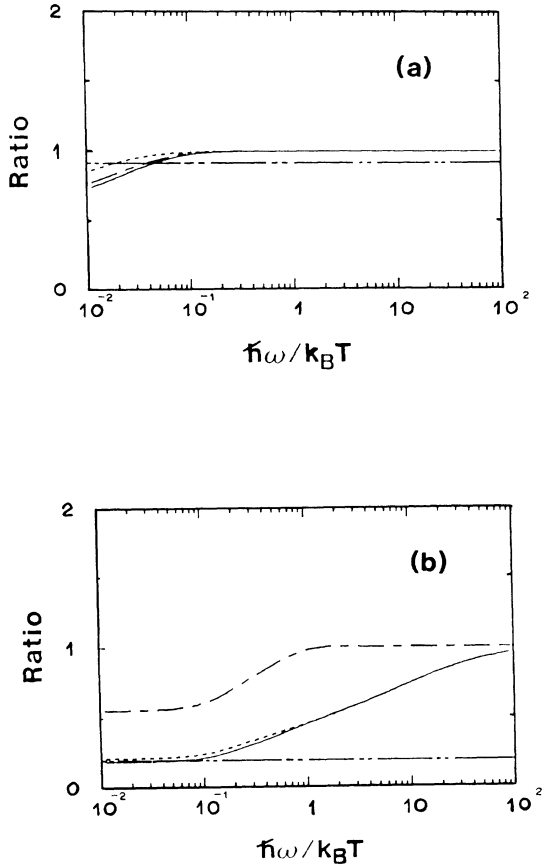

FIG. 11. (a) Ratios $R(\omega)$, $R_e(\omega)$, and $R_i(\omega)$ for case (a). ——, $R(\omega)$; · · · ·, $R_e(\omega)$; and —·—·—·, $R_i(\omega)$. $(Z^*/Z)^2$ is shown by –··–. (b) Same as (a) for case (b).

determined by $1/q_{\max}$, where $q_{\max}$ is the maximum point of the integrand $S(q)P(q)F(q)/q$ in Eq. (3). The value of $q_{\max}$ is approximately equal to the maximum of $F(q)$, which is indicated by arrows in Figs. 9(a) and 9(b) and scaled by $q_{\max}\sim(2m\omega/\hbar)^{1/2}$. When the impact parameter is small, the electron which interacts with the radiation feels almost bare Coulomb potential Ze/r (larger than Z^*e/r) and therefore $S(q)=P(q)=1$ effectively. Therefore when $\hbar\omega$ is larger than k_BT, $R(\omega)$ is larger than $(Z_*/Z)^2$ and approaches unity for $\hbar\omega\rightarrow\infty$. In the case of the large impact parameter, the colliding electron feels the modified Coulomb potential which is determined by the effects of the ion-ion correlation and the bound and free electron shieldings. As for the effects of the bound electron shielding, we can take it into account by using the potential Z^*e/r effectively. So when $\hbar\omega$ is small and the bound electron shielding effects are dominant, $R(\omega)$ approaches to $(Z^*/Z)^2$ in Fig. 11(b). When the plasma approaches to the fully ionized state, namely, Z^* is nearly equal to Z, the effects of the ion-ion correlation and the free-electron shielding are large and $R(\omega)$ becomes smaller than $(Z^*/Z)^2$ at small $\hbar\omega$ as shown in Fig. 11(a).

In this work we have studied the effects of the ion-ion correlation and the electronic screening on the bremsstrahlung. The influence of these effects may be observed in the numerical simulation of laser plasmas. The dominant contribution of the radiation to the energy transport is determined by the absorption coefficient at $\hbar\omega\sim k_BT$. In the typical laser plasma parameter, $Z=13$, $n_i=8\times10^{22}$ cm^{-3}, and $k_BT=100$ eV, corresponding to case (b), the ratio $R(\omega)$ largely changes at $\hbar\omega\sim k_BT$ by the effects of the ion-ion correlation and the electronic screening as shown in Fig. 11(b), indicating that the radiation transport in the laser plasmas is sensitive for these effects.

ACKNOWLEDGMENTS

The authors thank Dr. H. Takabe and S. Kato at the Institute of Laser Engineering (ILE), Osaka University and Professor Y. Furutani at the Department of Electronics, Okayama University for discussions and encouragement. This work was partially supported by the Grant-in-Aid for Scientific Researches from the Ministry of Education, Science and Culture of Japan.

[1]H. Totsuji, Phys. Rev. A **32**, 3005 (1985).
[2]R. M. Moore, *Atomic Physics in Inertial Confinement Fusion* (Lawrence Livermore Laboratory, Livermore, 1981), Sec. III-B.
[3]R. Latter, Phys. Rev. **99**, 1854 (1955).
[4]F. Perrot, Phys. Rev. A **35**, 1235 (1987).
[5]V. B. Berestetskii, E. M. Lifshitz, and L. P. Pitaevskii, *Relativistic Quantum Theory* (Pergamon, Oxford, 1971), Pt. 1, Sec. 45.
[6]H. Totsuji and K. Tokami, Phys. Rev. A **30**, 3175 (1984).
[7]Kin-Chue Ng, J. Chem. Phys. **61**, 2680 (1974).
[8]S. Yamaguchi, S. Kawata, T. Abe, and K. Niu, Research Report of the Institute of Plasma Physics (Nagoya, Japan) No. IPPJ-553, 1982 (unpublished).